NeuroImage: Clinical 21 (2019) 101606

Contents lists available at ScienceDirect

NeuroImage: Clinical

journal homepage: www.elsevier.com/locate/ynicl

Contributions of a high-fat diet to Alzheimer's disease-related decline: A longitudinal behavioural and structural neuroimaging study in mouse models

Colleen P.E. Rollins[a,e,*,1], Daniel Gallino[a], Vincent Kong[a,b], Gülebru Ayranci[a], Gabriel A. Devenyi[a,c], Jürgen Germann[a], M. Mallar Chakravarty[a,b,c,d,*]

[a] Computational Brain Anatomy Laboratory, Cerebral Imaging Centre, Douglas Mental Health University Institute, Montreal, Quebec H4H 1R3, Canada
[b] Integrated Program in Neuroscience, McGill University, Montreal, Quebec H3A 2B4, Canada
[c] Department of Psychiatry, McGill University, Montreal, Quebec H3A 1A1, Canada
[d] Department of Biological and Biomedical Engineering, McGill University, Montreal, Quebec H3A 2B4, Canada
[e] Department of Psychiatry, University of Cambridge, Herchel Smith Building, Cambridge CB2 0SP, United Kingdom

A B S T R A C T

Obesity is recognized as a significant risk factor for Alzheimer's disease (AD). Studies have supported that obesity accelerates AD-related pathophysiology and memory impairment in mouse models of AD. However, the nature of the brain structure-behaviour relationship mediating this acceleration remains unclear. In this manuscript we evaluated the impact of adolescent obesity on the brain morphology of the triple transgenic mouse model of AD (3xTg) and a non-transgenic control model of the same background strain (B6129s) using longitudinally acquired structural magnetic resonance imaging (MRI). At 8 weeks of age, animals were placed on a high-fat diet (HFD) or an ingredient-equivalent control diet (CD). Structural images were acquired at 8, 16, and 24 weeks. At 25 weeks, animals underwent the novel object recognition (NOR) task and the Morris water maze (MWM) to assess short-term non-associative memory and spatial memory, respectively. All analyses were carried out across four groups: B6129s-CD and -HFD and 3xTg-CD and -HFD. Neuroanatomical changes in MRI-derived brain morphology were assessed using volumetric and deformation-based analyses. HFD-induced obesity during adolescence exacerbated brain volume alterations by adult life in the 3xTg mouse model in comparison to control-fed mice and mediated volumetric alterations of select brain regions, such as the hippocampus. Further, HFD-induced obesity aggravated memory in all mice, lowering certain memory measures of B6129s control mice to the level of 3xTg mice maintained on a CD. Moreover, decline in the volumetric trajectories of hippocampal regions for all mice were associated with the degree of spatial memory impairments on the MWM. Our results suggest that obesity may interact with the brain changes associated with AD-related pathology in the 3xTg mouse model to aggravate brain atrophy and memory impairments and similarly impair brain structural integrity and memory capacity of non-transgenic mice. Further insight into this process may have significant implications in the development of lifestyle interventions for treatment of AD.

1. Introduction

The rising prevalence of Alzheimer's disease (AD), the most common form of dementia, distinguishes it as a worldwide healthcare concern (Livingston et al., 2017). Importantly, the neurobiological mechanisms that elevate risk for AD may be occurring years and potentially decades before an actual diagnosis. Recent epidemiological studies have identified potentially modifiable lifestyle features such as diabetes, hypertension, obesity, smoking, late-life depression, low educational attainment, and physical inactivity as significant risk factors for AD

Abbreviations: AD, Alzheimer's disease; 3xTg, triple transgenic mouse model of AD; B6129s, Non-transgenic control mice of the same background strain; HFD, high-fat diet; CD, control diet; MWM, Morris water maze; NOR, novel object recognition; MRI, magnetic resonance imaging

* Corresponding authors at: Computational Brain Anatomy Laboratory (CoBrA Lab) Cerebral Imaging Centre, Douglas Mental Health University Institute, 6875 LaSalle Boulevard, Montreal, Quebec H4H 1R3, Canada

E-mail addresses: colleen.rolllins2@mail.mcgill.ca (C.P.E. Rollins), mallar@cobralab.ca (M.M. Chakravarty).

[1] Department of Psychiatry, Herchel Smith Building, University of Cambridge, Robinson Way, Cambridge CB2 0SP, United Kingdom.

https://doi.org/10.1016/j.nicl.2018.11.016
Received 9 March 2018; Received in revised form 26 July 2018; Accepted 18 November 2018
Available online 20 November 2018

(Barnes and Yaffe, 2011; Livingston et al., 2017). Importantly, an accumulation of evidence has recognized that obesity, in particular, can increase the risk of AD later in life independently of other risk factors (Profenno et al., 2010; Whitmer et al., 2008; Xu et al., 2011; Kivipelto et al., 2006; Bischof and Park, 2015). Obesity seems to act not only synergistically with aging, but, in fact, as an agent that accelerates brain alterations and cognitive impairment related to aging, adding an estimated increase of brain age of 10 years (Ronan et al., 2016). For instance, obesity, as measured by higher body mass index (BMI), has been associated with patterns of lower regional brain volume (Bobb et al., 2014) and cognitive decline (Bischof and Park, 2015) from adolescence/early adulthood (Yau et al., 2012) into healthy aging. Moreover, higher BMI has been associated with brain atrophy in the anterior hippocampus in patients with AD (Ho et al., 2011; Ho et al., 2012), suggesting that obesity may accelerate the neurodegenerative trajectories towards AD by impacting critical brain areas that appear to be preferentially preserved in healthy aging (Tardif et al., 2018; Amaral et al., 2016; Voineskos et al., 2015; de Flores et al., 2015).

Though much of the link between obesity and dementia has been explored with regards to obesity in midlife, there is evidence that obesity during childhood and adolescence may equally contribute to later life cognitive impairment, dementia, and AD (Seifan et al., 2015; Luciano et al., 2015). Importantly, obesity during adolescence is also an excellent predictor of obesity later in life (Simmonds et al., 2016), potentially compounding the influence of brain alterations from maturation to midlife. This is unsurprising considering that adolescence is a critical period for brain maturation. Disturbances to brain development during this time, such as those induced by obesity (Yau et al., 2012) and other early-life environmental factors (Moceri et al., 2000), may have long lasting effects on brain structures important in the pathogenesis of AD. The hippocampus undergoes substantial alterations during adolescence and might be particularly vulnerable to diet-mediated alterations in brain development (Hueston et al., 2017). In mice, consumption of a high-fat diet (HFD) from adolescence to adulthood worsens memory flexibility and decreases hippocampal neurogenesis, to even a greater degree than adult consumption of the same diet (Boitard et al., 2012), supporting evidence suggesting a heightened sensitivity to the effects of HFD on memory during the adolescent period. In humans, consumption of high-fat foods during adolescence is associated with neurostructural and cognitive deficits (Reichelt, 2016; Reinert et al., 2013). Not only may obesity in adolescence have enduring consequences on brain structure and cognition, but lifestyle habits, such as dietary choices, developed in adolescence may determine adult health patterns (Sawyer et al., 2012). Indeed, obesity in childhood and adolescence is strongly associated with increased risk of severe obesity in adulthood (The et al., 2010), as well as increased risk of diabetes, metabolic syndrome (Biro and Wien, 2010), and depression (Reichelt, 2016), which in themselves constitute risk factors for AD (Alford et al., 2017). Alarmingly, the global prevalence of overweight and obesity combined has increased by 27.5% for adults and 47.1% for children in the last 3 decades, with a current estimated prevalence of 23% of children and adolescents (aged 2–19) being either overweight or obese in developed countries (Ng et al., 2014). Considering the dramatic inflation in diet-mediated obesity in early life, it is critical to establish how obesity might affect brain structure and function in the long term, especially with regards to trajectories towards AD-related decline, in order to address the double epidemic of obesity and Alzheimer's disease.

As high-fat, energy-dense meals are a main contributor to obesity (Guyenet and Schwartz, 2012), the contribution of obesity to enduring deficits in adolescent cognition, brain structure, and subsequent risk for AD can be directly investigated with HFD induced obesity in young mouse models of AD (as a proxy for a high-risk group). Previous studies have demonstrated that risk factors for AD may influence brain structure at birth (Dean 3rd et al., 2014) and the adolescent period (Shaw et al., 2007). Therefore a nuanced understanding of how AD-related trajectories are impacted by obesity is critical to reducing AD-related risk.

Animal studies using this paradigm have found increases in amyloid-beta (Aβ) protein and soluble tau (Vandal et al., 2014; Barron et al., 2013; Petrov et al., 2015; Julien et al., 2010), but these findings are not consistent between groups, with some studies reporting no change in levels of Aβ or tau (Knight et al., 2014; Gratuze et al., 2016). A major limitation of much of the literature on obesity in mouse models of AD is the wide methodological variation in mice strain, length of time maintained on diet, differing amounts of fat in the diet, or lack of appropriate controls for transgenic strain or diet. Importantly, these inconsistencies highlight the need to clarify how obesity may modulate neurodegenerative trajectories towards cognitive decline and the onset of AD. Moreover, no pre-clinical studies have used magnetic resonance imaging (MRI; as has been done in the clinical literature) to assess structural changes in the brain associated with obesity in the context of AD. Thus, a longitudinal analysis considering changes in body weight, brain structure, and their correlation with behaviour, is required to better establish this association between obesity and increased risk for AD later in life.

The current study determines the impact of high-fat diet mediated obesity on brain structure and behaviour of the triple transgenic mouse model of AD (3xTg) and non-transgenic control mice (B6129s) using a longitudinal design. With regards to the current body of research, we hypothesize that high-fat feeding in adolescence will accelerate the structural changes associated with AD and impair memory in 3xTg and B6129s control mice.

2. Materials and methods

2.1. Animals and dietary treatment

All animal experiments were carried out in accordance with the Canadian Council on Animal Care and approved by the McGill University Animal Care Committee (Montreal, QC, Canada). Male and female homozygous 3xTg mice (https://www.jax.org/strain/004807, RRID:MMRRC_034830-JAX) were originally acquired through Mutant Mouse Resource and Research Center (MMRRC) and were bred from an in-house colony. Harbouring the PS1M146V, APPSwe, and tauP301L transgenes, the 3xTg model progressively exhibits Aβ deposition into plaques, tau tangle pathology, synaptic dysfunction, and age-dependent cognitive impairment that correlate with Aβ accumulation (Oddo et al., 2003a, 2003b; Eriksen and Janus, 2007). These changes are similar to human AD pathology and offer a more comprehensive model of AD in comparison to other animal models used that display only a subset of these features. Moreover, the longitudinal trajectories of brain structure and behaviour have been well characterized in this model (Kong et al., 2018). The non-transgenic control mice used here (B6129s) were offspring of F2 hybrid mice from a cross between C57BL/6 J females (B6) and 129S1/SvImJ males (129S), the same background as the 3xTg mice (https://www.jax.org/strain/101045, RRID:IMSR_JAX:101045). Animals were bred and housed at the Douglas Mental Health University Institute's Animal Facility (Montreal, QC, Canada) in standard housing conditions (12 h light/dark cycle, with lights on at 08:00) in groups of up to 4 mice per cage, with ad libitum access to standard chow and water. At the age of 8 weeks, animals were weighed (Week 0 on diet) and placed on either a HFD (60.3% kcal from fat, TD.06414, Envigo Teklad Diets, Wisconsin, USA, http://www.envigo.com/resources/data-sheets/06414.pdf) or on an ingredient-equivalent low-fat control diet (10.5% kcal from fat, TD.08806, Envigo Teklad Diets, Wisconsin, USA, http://www.envigo.com/resources/data-sheets/08806.pdf), depending on their group, and were maintained on the diet for the remainder of the experiment. Supplementary Tables A1 and A2 list the nutrient and ingredient information for each diet, respectively. Animals were weighed daily for the first 5 days following dietary change to ensure that they were able to adhere to the new diet and were not losing

Table 1
Number of animals per group for each experimental procedure.

Age (weeks)	Procedure	Group			
		3xTg-HFD	3xTg-CD	B6129s-HFD	B6129s-CD
8	MRI	10 (2 M/8F)	10 (6 M/4F)	9 (4 M/5F)	9 (6 M/3F)
16	MRI	10 (2 M/8F)	10 (6 M/4F)	9 (4 M/5F)	9 (6 M/3F)
24	MRI	10 (2 M/8F)	10 (6 M/4F)	9 (4 M/5F)	9 (6 M/3F)
25	NOR	10 (2 M/8F)	10 (6 M/4F)	8 (4 M/4F)	9 (6 M/3F)
25–26	MWM	9 (2 M/7F)	10 (6 M/4F)	8 (4 M/4F)	8 (5 M/3F)

Abbreviations: 3xTg: triple transgenic mice; B6129s: non-transgenic control mice; HFD: high-fat diet; CD: control diet; MRI: magnetic resonance imaging; NOR: novel object recognition task; MWM: Morris water maze.

weight, and were weighed weekly for the remainder of the experiment. Table 1 illustrates the number of animals per group for each experimental procedure. 2 animals passed during the final week of the experiment (see Table 1).

2.2. Magnetic resonance image acquisition

All experiments were performed on 7.0-T small animal scanner (Bruker Biospec 70/30 USR; 30-cm inner bore diameter) at the Douglas Mental Health University Institute (Montreal, QC, Canada). Animals were imaged in vivo at each of 3 time points: 8 weeks of age (time point 1); 16 weeks of age (time point 2) and 24 weeks of age (time point 3). These timepoints were chosen based on the expected pathological evolution typically expected in 3xTg's (Oddo et al., 2003a, 2003b; Kong et al., 2018): week 8 precedes known pathological accumulation, weeks 12–16 marks the initial accumulation on intracellular AB peptide, and week 24 marks the initiation of extracellular AB peptide and impaired spatial working memory.

Immediately prior to each scanning session, animals were anaesthetized with isoflurane (Fresenius Kabi Canada Ltd., Richmond Hill, CA) at 5% and were injected subcutaneously with 0.5 mL of 0.9% sterile sodium chloride physiological solution (saline) (Sigma Aldrich, Buchs, Switzerland). During scanning, animals were maintained under 1–2% isoflurane, with breathing rate monitored and maintained at 30–100 breaths per minute. 3-dimensional fast low angle shot (3D FLASH) T1-weighted MRIs were taken with 2 averages (TR = 20 ms, TE = 4.5 ms, matrix size = 180 × 160 × 90, voxel dimensions = 100 μm isotropic, flip angle = 20°) with the Bruker 23 mm volumetric transmit/receive quadrature coil. The parameters were chosen to optimize the resolution and contrast of the scan and to bring the total imaging time to ~14 min. 24 h prior to each imaging session, mice were injected with a manganese (II) chloride ($MnCl_2$) solution (Lee et al., 2005) at a dosage of 62.5 mg/kg to enhance the contrast of T1 structural MRI scans (Silva and Bock, 2008; Massaad and Pautler, 2011; Malheiros et al., 2015). The solution of $MnCl_2$ was made by injecting 0.313 mL of 1 M $MnCl_2$ (Sigma Aldrich, Buchs, Switzerland) into 10 mL of saline. Injections prior to the second (16 weeks) and third (24 weeks) scan were calculated according to the animal's initial body weight measured at 8 weeks of age to prevent the administration of high doses of $MnCl_2$ that would have been necessitated by HFD-induced body weight increases. This was done since during initial pilot experiments, an increased incidence of risk of skin lesions was observed in animals when the dose administered was increased in proportion to HFD-elevated body weight (data not shown). Since high doses of $MnCl_2$ have been shown to induce systemic toxicity in mice, the injection method (subcutaneous or intraperitoneal) was changed at different time points in order to minimize potential tissue damage that could incur from repeated injections at the same location (Poole et al., 2017). Importantly, differences in injection route have not been shown to affect T1 scan contrast. Kuo et al. (2005) conducted a systematic review on pharmacokinetic differences in the enhancement of T1 relaxation in brain regions following $MnCl_2$ administration either by intravenous (IV), intraperitoneal (IP), or subcutaneous (SC) injections at 9.4 T and found no significant differences in mean T1 times at 24 h post-injection. The $MnCl_2$ solution was modified partway through the experiment with the addition of 1 M sodium hydroxide (NaOH) (Sigma Aldrich, Buchs, Switzerland) in order to reduce the slightly acidic nature of manganese, namely tissue damage at the site of injection. The NaOH maintained the pH of the solution near 7.4 (Seo et al., 2011), while maintaining the $MnCl_2$ concentration constant. The effects of the manganese dose, administration route, and NaOH modification on the quality of the acquired MRI brain images were compared qualitatively by visual inspection. It should be noted that complications due to $MnCl_2$ administration have previously been observed and reported in Vousden et al. (2018). No differences of anatomical contrast between groups were observed (data not shown). All scans were visually inspected in the Display visualization software of MINC tools (http://www.bic.mni.mcgill.ca/ServicesSoftwareVisualization/Display, RRID:SCR_014138) to check for scanner artifacts and gross neuroanatomical abnormalities.

2.3. Behavioural tests

Animals underwent the novel object recognition (NOR) and Morris water maze (MWM) tests to assess short-term non-associative memory and spatial reference memory, respectively. 1 week following their third MRI scan (24 weeks), animals were tested with the NOR (2 days duration) and 1 day later the MWM (7 days duration) began. No > 1 testing session occurred on any given day in order to minimize stress to the mouse. On each test day, home cages were brought to the testing rooms 30 min prior to the beginning of the test to acclimatize the animals to the room.

2.3.1. Novel object recognition

On day 1 of NOR, mice were placed in a cubic open field box (45 cm^3) with a small amount of bedding from their home cage to habituate them to the arena and were allowed to freely explore for 10 min. On day 2 of NOR, animals were again placed in the same box with a small amount of home bedding and were allowed to explore 2 identical objects (approx. 4 cm^3), spaced 25 cm apart for 10 min. Mice were then removed and returned to their home cages in the test room. 1 h later, animals were returned to the same box with 1 of the objects replaced with a novel object. Mice were again allowed to explore the objects for 10 min. The location of the novel object as appearing on the right or left size was randomized and balanced across trials. The box and objects were thoroughly cleaned between trials. The test room was under red light and an overhead camera was used to capture behaviour. The resultant MP4 video clips were converted to Windows Media Video (WMV) by Windows Media Player to enhance contrast. The amount of time spent exploring each object, number of bouts of exploring each object, and speed of the animal was tracked by the TopScan 2.0 behavioural analysis system (Clever Sys Inc., Reston, Virginia). Exploration was defined as the amount of time the animal spent with their nose pointing within 2.5 cm of the object (as suggested by the internal protocol of the Douglas Mental Health University Institute). The discrimination ratio (M) was calculated as the amount of time spent

exploring the novel object (Fn) minus the amount of time spent exploring the familiar object (Ff) divided by the total amount of time spent exploring both objects (Fn + Ff). A discrimination ratio of 0 suggests that the animal has no ability to discriminate a novel object and thus has poor short-term memory, a negative discrimination ratio indicates that the animal spent more time exploring the familiar object compared to the novel object.

2.3.2. Morris water maze

Morris water maze was performed in a 120 cm diameter circular tank containing water (21–22 °C) made opaque by the addition of white non-toxic tempera paint. 3 visual cues were placed on the interior wall of the tank above the water line (N, E, SW). A 15 × 15 cm escape platform was submerged 1 cm below the surface of the water. The MWM consisted of 1 habituation day, 5 training days, and 1 probe day. On the first day (day 0), animals underwent 1 trial of visual platform training, wherein the platform was visible (1 cm above the surface of the water). This was done to habituate the animals to the pool and to test for visual acuity deficits. On training days (day 1–5), the platform was located in the SW quadrant and animals underwent 6 trials, entering from 1 of 3 start points (NE, SW, SE) in pseudorandom order. Supplementary Table A3 illustrates trial start points and platform locations for each day of the water maze. If mice did not find the platform within 60 s, they were gently guided towards it. A failure was defined as a trial in which the mouse did not find the platform within 60 s. After each trial, mice were returned to their home cage for an inter-trial time of 10 min. To test the memory retention of the platform location, a probe trial was performed (day 6), in which the platform was removed. Mice underwent 1 trial for the probe and were allowed 60 s to explore. Each trial was monitored using a camera mounted directly above the pool and analyzed using tracking software (HVS Water 2100, HVS Image Ltd., Buckingham, UK). The following parameters were recorded by the tracking software each day and were retained for analysis: Escape latency (s), % time spent (s) and % distance travelled (m) in each quadrant, pathlength to the platform (m), swim speed (m/s), time spent floating (s), and % time spent (s) near the platform location (within 2 cm of platform boundaries, probe day only; this distance was chosen based on options available in the tracking software).

2.4. Deformation-based analysis

A deformation-based analysis was performed using the two-level registration pipeline from Pydpiper (Friedel et al., 2014) (https://wiki.mouseimaging.ca/display/MICePub/twolevel_model_building) to assess longitudal voxel-wise changes in brain volume in all subjects. In contrast to other group-wise registration paradigms, the main advantage of this methodology is that it uses nonlinear registration to align images from all time points for a given subject to a subject-specific consensus model, in addition to a population-specific average. This enables comparison of neuroanatomical changes in a given subject across all time points. Briefly, the two-level registration approach proceeds as follows: all subject scans were linearly registered to a common coordinate space via rigid (6-parameter) alignment and subsequently underwent pairwise affine (12-parameter) registration to compute the average transform for all pairs. Transformations were applied to each MRI image and the outputs were averaged using an iterative group-wise procedure to create a 12-parameter population-specific atlas (LSQ12 atlas). Each mouse brain was nonlinearly registered to the LSQ12 atlas using Advanced Normalization Tools (ANTs) registration (Avants et al., 2008, 2011) to create a second atlas, which was used as the target for subsequent nonlinear registration steps. This method has been described in Friedel et al. (2014) and Kong et al. (2018) and cross-sectionally by Chakravarty et al. (2016) and Allemang-Grand et al. (2017). Subject-specific averages were then registered to create a final nonlinear population-specific average. Transforms mapping from the common space group average to each subject specific average and to each individual scan were then calculated to determine the deformation fields. Finally, the log-transformed Jacobian determinant (Chung et al., 2001), a measure of relative voxel-wise expansion and contraction, was calculated at each voxel in the deformation fields and was blurred with Gaussian smoothing using 0.2 mm full width at half maximum kernel. Quality control of the two-level registration was performed by visually assessing the resultant images of both the first and second level registrations for proper orientation, size, and sensible subject-specific averages. The resulting blurred Jacobians were subsequently input into our statistical analyses (see below) as the dependent variable.

2.5. Volumetric analysis

All MRI images were converted from DICOM to MINC format. Scan preprocessing steps included axis orientation correction, orientation correction, denoising (Manjon et al., 2010), creation of a approximate brain mask by registration to an atlas, and bias field calculation and correction with N4 (Tustison et al., 2010). To assess whether HFD-induced obesity was associated with brain volume alterations in 3xTg mice, MRI images were first segmented into 159 structures per hemisphere using the Multiple Automatically Generated Templates (MAGeT) brain segmentation algorithm (Chakravarty et al., 2013). MAGeT brain works by generating a template library from a subset of target images and producing multiple segmentations for each subject via pairwise nonlinear image registration. Final segmentations for each subject are determined by a majority-vote label fusion method. Quality control of the resultant segmentations was performed by visual inspection of overlaying the final segmentations atop each subject image to ensure the labels matched the underlying anatomy. Brain regions were labeled using the Dorr-Steadman-Ulman atlas (Mouse Imaging Centre, The Hospital For Sick Children, Toronto, CA) (Dorr et al., 2008; Steadman et al., 2014; Ullmann et al., 2014) and their volumes were computed from these segmentations. Select regions were hierarchically grouped into more coarser-grained labels (e.g.: Caudomedial entorhinal cortex, Dorsal intermediate entorhinal cortex, Dorsolateral entorhinal cortex, Dorsal tenia tecta, Medial entorhinal cortex, Ventral intermediate entorhinal cortex, and Ventral tenia tecta were grouped as Entorhinal cortex) due to the limitations of the MRI image resolution and contrast. Label groupings were based on the hierarchical anatomical labeling described in Supplementary Table A4.

2.6. Statistical Analysis

Throughout the remainder of this manuscript all analyses will take place using four different groups: B6129s-HFD, B6129s-CD, 3xTg-HFD, and B6129s-CD. All statistical analyses were performed using these group definitions unless otherwise stated.

2.6.1. Body weight and behavioural analysis

Body weight and MWM training data were analyzed with 2-way repeated measures ANOVAs. For body weight, group was included as a between-subjects factor and week as the within-subjects factor, with sex included as a covariate to control for expected differences in weight between male and female animals. For MWM training (days 1–5), the interaction between group (between-subjects) and training day (within-subjects) on latency and path length to reach the platform was explored. For the MWM probe day, a 1-way ANOVA was used to assess the effect of experimental group on the percent time spent in the target quadrant (ie., the quadrant that previously held the platform), percent total path length spent in the target quadrant, and percent total time spent near the platform location, respectively. Swim speed was included as a covariate in all MWM ANOVAs in order to control for expected differences between high-fat fed and control fed animals. The chi-square test (χ^2) was used to detect group differences in the number of failures to find the platform on MWM training days on a per day

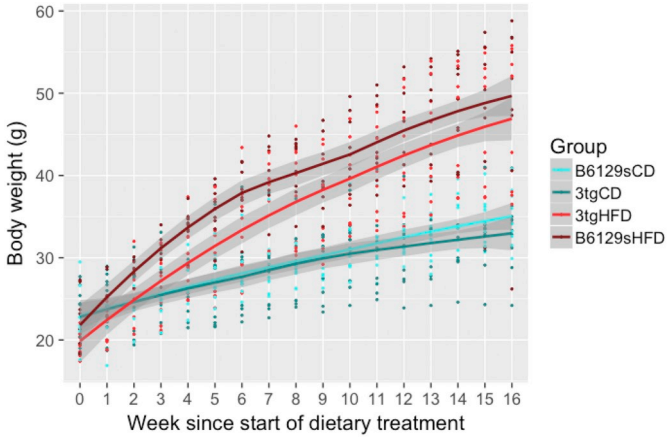

Fig. 1. High-fat feeding increases body weight in all animals. All mice (both males and females) were maintained on either a control diet (CD) or high-fat diet (HFD) from 8 weeks of age (week 0 in figure). A 2-way repeated measures ANOVA was conducted, followed by Tukey HSD post-hoc testing. B6129s mice maintained on the HFD had greater body weights than B6129s and 3xTg mice fed the CD from their fourth week on the diet onwards, while 3xTg mice on the HFD were heavier than all mice on the CD from their sixth week on the diet onwards. The error bars represent the standard error of the mean and the shaded gray areas represent the 95% confidence level interval. There were no differences between genotypes for high-fat or control-diet fed mice. * $p < .05$, ** $p < .01$, *** $p < .001$ B6129s mice on HFD versus 3xTg and B6129s mice on CD; # $p < .05$, ## $p < .01$, ### $p < .001$ 3xTg on HFD versus 3xTg and B6129s mice on CD.

basis. The learning curve for each mouse across MWM training was modelled using an exponential decay function. The learning curve graphically represents the rate of improvement on a task in which performance improves as a function of practice, with a beta coefficient of 1 indicating no learning and a lower beta coefficient indicating better learning. The beta coefficients of the learning curves for latency and path length to platform were analyzed with a 1-way ANOVA. Trials in which a mouse failed to find the platform were excluded from calculating the coefficients of the path length learning curves. Data from the NOR task was also analyzed with a 1-way ANOVA to examine the effect of experimental group on discrimination ratio. Tukey HSD was used for all post-hoc testing. Statistical significance was set at a threshold of $p < .05$. The ANOVA function in R did not report exact p-values < .001, nor did the Tukey HSD function for p-values < .01. In all other cases p-values are reported with three significant figures.

2.6.2. Volumetric and deformation-based analyses

Linear mixed effects models were used here as they correctly model the interrelationships in the data that occur by having multiple time points and are appropriate for longitudinal analyses as they can deal with data with missing values (Bernal-Rusiel et al., 2013). Differences in longitudinal trajectories were modelled using group, time point, and sex included as fixed effects and subject-specific intercepts and age (in weeks) included as random effects. The model treated time point as a quadratic term and included an interaction between group and time point. Though many studies model time as linear due to its conceptual simplicity and interpretability, a linear trajectory of brain structure assumes that the rate of growth or decline remains constant over time, an assumption that should be questioned considering the accelerated volume changes in older age that are best modelled by quadratic fits in both humans and mice (Pfefferbaum et al., 2013; Ziegler et al., 2012; Kong et al., 2018) and the complex interactions with modifiers of brain aging like obesity and disease. In contrast, higher-order polynomial trends, such as a quadratic slope, indicate that growth rates might not be the same over time. For this reason, time point was chosen to be modelled as a quadratic term to provide a more flexible and accurate model of brain volumetric trajectories across age and genotype. Age was included as a random effect in order to account for small variation in age at each time point from the per-subject results. This LME model was used in the analysis of MAGeT-derived volumes of brain structures, as well as for the voxel-wise analysis of the log-transformed absolute Jacobians. False discovery rate (FDR) was used for multiple comparison correction with a 5% threshold.

Further analyses were performed in the two genotype groups (3xTg and B6129s) separately, as well as in the two dietary treatment groups (CD and HFD), in order to dissect the specific effect of high-fat feeding in 3xTg and B6129s mice, as well as the specific effect of transgenic status in mice maintained on the HFD and CD. LME models for these analyses included the interaction between time point (quadratic) and diet for the genotype subgroups and the interaction between time point (quadratic) and genotype for the diet subgroups.

Moreover, analyses were performed to examine voxelwise associations between neuroanatomical volume and behavioural measures using a LME model relating the normalized Jacobian determinant derived from the mouse's third MRI scan to each of: the NOR discrimination ratio, the percent time spent in the target quadrant during the MWM probe trial, the percent of the mouse's path spent in the target quadrant during the MWM probe trial, and the percent of time spent near the prior platform location during the MWM probe trial.

All data are presented as mean +/− SEM and were analyzed in the R environment (RStudio, RRID:SCR_000432, v.3.2.4). RMINC 1.4.4.0 (Lerch et al., 2016) was used to integrate voxel-based statistics for MINC volumes into the R environment, the lme, lme4 and lmerTest packages employed for LME modeling, the multcomp package was used for the post-hoc Tukey's test, and plots and figures were generated with ggplot2.

3. Results

3.1. High-fat feeding increases body weight in all mice

High-fat feeding induced robust weight gain in all animals (3xTg and B6129s) maintained on the HFD (Fig. 1). At 8 weeks of age (week 0 of dietary treatment), there were no significant differences in weight between groups. A 2-way repeated measures ANOVA revealed a significant interaction between group and week ($F(3, 604) = 183.845$, $p < .001$). The main effect of group, week, and sex were also significant (group $F(3,33) = 17.198$, $p < .001$; week ($F(1,604) = 3223.667$, $p < .001$; sex $F(1,33) = 8.459$, $p = .00653$). Tukey HSD post-hoc testing showed that B6129s-HFD mice had greater body mass compared to 3xTg and B6129s mice on the CD from week 4 onwards (B6129s-HFD - 3xTg-CD $p = .00026$; B6129s-HFD - 3xTg-HFD $p = .00037$), while the 3xTg mice on the HFD had greater body mass than the 3xTg and B6129s mice on the CD from week 6 onwards (3xTg-HFD - 3xTg-CD $p = .0468$; 3xTg-HFD - B6129s-CD $p = .0109$). There were no differences in body mass within dietary groups (ie., between 3xTg or B6129s mice on the CD or HFD) at any week.

3.2. HFD in control mice diminishes novel object recognition towards the level of 3xTg mice

At 25 weeks of age, a significant effect of group on discrimination ratio was observed (ANOVA, $F(3,33) = 3.421$, $p = .0284$), such that 3xTg mice fed the HFD exhibited impaired performance on novel object recognition in comparison to the B6129s mice maintained on the CD (Tukey HSD, $p = .0271$) (Fig. 2). While the B6129s-CD mice showed a robust preference for the novel object (M = 0.26), all other groups had no or little preference for the novel object and explored both the novel and familiar objects to a similar degree (B6129s-HFD M = 0.07; 3xTg-CD M = 0.02; 3xTg-HFD M = −0.05). Contrary to our hypothesis, high-fat feeding did not significantly impair memory within genotype subgroups, though it did worsen performance in the B6129s-HFD

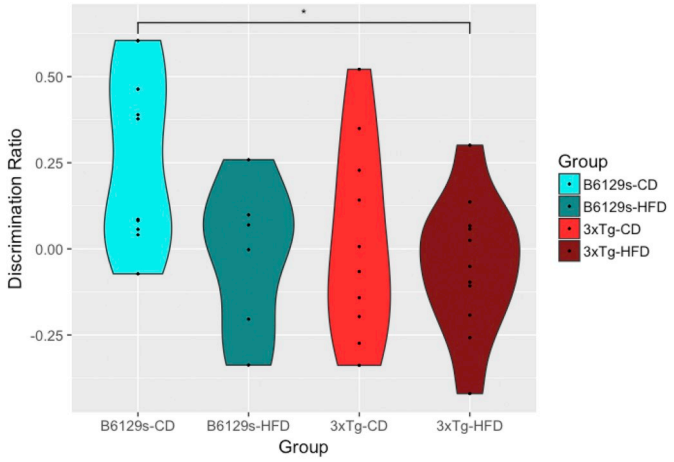

Fig. 2. Group-wise discrimination ratios on the NOR task. All mice were maintained on either a control diet (CD) or high-fat diet (HFD) from 8 to 26 weeks of age. Short-term non-associative memory was assessed with the novel object recognition task at 25 weeks of age. A 1-way ANOVA was conducted, followed by Tukey HSD post-hoc testing. Impaired performance in novel object recognition was observed in 3xTg mice fed the HFD in comparison to B6129s mice maintained on the CD. 1 outlier was removed from the B6129s-HFD group, though this did not change significance levels. * $p = .02710$ B6129s-CD - 3xTg-HFD.

control mice. There were no differences for speed or total distance travelled between groups, nor were there group differences in overall levels of exploration, though levels of exploration were low among all animals (< 30%).

3.3. HFD exacerbates memory impairments in 3xTg mice on specific MWM indexes

There were no significant differences in escape latencies between groups on the MWM visual platform training (day 0).

For MWM training days (1-5), all groups were able to learn the location of the hidden platform, as indicated by an overall reduction in escape latency and path length across training days (Fig. 3a and b, respectively). Within groups, B6129s and 3xTg mice maintained on the CD showed significantly reduced escape latencies and path lengths across all training days (2-way repeated measures ANOVA, $F(19, 125) = 15.306$, $p < .001$). B6129s mice under high-fat feeding showed reduced escape latencies on days 3–5 compared to day 1 (Tukey HSD, day 3 - day 1 $p < .01$, day 4 - day 1 $p < .01$, day 5 - day 1 $p < .01$) and on day 5 compared to day 2 (Tukey HSD, $p = .0327$) and reduced path lengths on day 5 compared to days 1 and 2 (day 5 - day 1 $p < .01$, day 5 - day 2 $p < .01$). 3xTg mice under high-fat feeding showed reduced escape latencies on days 3–5 versus day 1 and 4–5 versus day 2 (Tukey HSD, day 3 - day 1 $p < .01$, day 4 - day 1 $p < .01$; day 5 - day 1 $p < .01$) and reduced path lengths on days 4 and 5 in comparison to day 2 (day 5 - day 2 $p < .01$; day 4 - day 2 $p < .01$). Between groups, 3xTg mice on the HFD had significantly greater escape latencies and path lengths than B6129s mice maintained on the CD on day 2 of MWM training (Tukey HSD, latency $p = .0441$, path length $p < .01$). Fig. 3e illustrates representative traces of swimming plots for each experimental group during MWM training days. Statistical analysis also revealed a significant effect of group on swim speed, such that the 3xTg-HFD group had significantly slower swim speeds than the B6129s-CD group on days 1–4 (Tukey HSD days 1–4 $p < .001$). The B6129s-HFD group was also significantly slower than the B6129s-CD group on days 2–3 (Tukey HSD day 2 $p < .001$, day 3 $p = .0166$) and the 3xTg-HFD group was slower than the 3xTg-CD group on day 2 (Tukey HSD, $p = .0487$).

The number of failures between groups were significantly different on training days 1–3 (day 1 $\chi 2(3, N = 4) = 8.0952$, $p = .0441$; day 2 $\chi 2(3, N = 4) = 11.727$, $p = .00838$; day 3 $\chi 2(3, N = 4) = 15.133$, $p = .00170$) (Fig. 3c). On day 1, 3xTg mice (HFD and CD) failed significantly more times to find the platform than B6129s mice (HFD and CD) (3xTg-HFD > B6129s-CD and B6129s-HFD; 3xTg-CD > B6129s-CD and B6129s-HFD). The same was true for day 2, though all mice maintained on the HFD had a higher number of failures than their genotype counterpart maintained on the CD (B6129s-HFD > B6129s-CD; 3xTg-HFD > 3xTgCD). By day 3, 3xTg mice on the HFD failed more times in finding the platform than B6129s mice (HFD and CD), as well as than 3xTg mice on the CD, suggesting that high-fat feeding exacerbated the memory impairments in the 3xTg mouse model of AD. There were no differences in failure rate on day 4 and no failures on day 5, indicating that all groups learned the location of the platform by the end of the training, but further suggesting that the learning rate was different between groups.

The B6129s-CD mice had significantly lower beta coefficients of the latency learning curves compared to the 3xTg-HFD group (Tukey HSD, $p = .00191$), indicating that they had a faster rate of learning. Notably, 3xTg mice maintained on the CD also had significantly lower beta coefficients than the 3xTg-HFD group (Tukey HSD, $p = .00966$), indicating that high-fat feeding reduced the rate of learning in 3xTg mice (Fig. 3d). The beta coefficients of the path length to platform learning curves were not statistically significant between groups, though the group trends were similar to those for the latency learning curves. The lack of significance may be due to the high number of trials excluded from the analysis due to failure to find the platform (Fig. 3c).

On the probe trial (day 6), 3xTg mice maintained on a HFD spent significantly less time swimming in the target quadrant (ie., in which the platform was previously held) than B6129s mice on the same diet (Tukey HSD, $p = .0429$) (Fig. 4a). 3xTg mice maintained on a CD spent significantly less time swimming in the target quadrant than B6129s control mice maintained on either the CD or HFD (Tukey HSD, 3xTg-CD - B6129s-CD $p = .0318$; 3xTg-CD - B6129s-HFD $p = .0378$). However, there was also a significant effect of swim speed, such that the 3xTg-HFD group swam significantly slower than the B6129s-CD group (Tukey HSD, $p = .00148$). Despite this, the results for path length were similar to those of time, with 3xTg mice on the CD traveling a significantly smaller portion of their path in the target quadrant compared to B6129s mice on the CD ($p = .0353$) (Fig. 4b). To obtain a more precise measure of subjects' spatial memory, we assessed group differences in the percent time spent within 2 cm of the previous platform location. This showed that 3xTg mice on the HFD spent significantly less time near the platform location than B6129s mice on the CD (Tukey HSD, $p \leq .01$) (Fig. 4c). Notably, there was a diet-specific effect within genotypes, such that 3xTg mice on the HFD spent significantly less time near the platform location than 3xTg mice on the CD and B6129s mice on the HFD performed worse than B6129s mice on the CD (Tukey HSD, 3xTg-HFD - 3xTg-CD $p = .0163$; B6129s-HFD - B6129s-CD $p = .0477$). There were no differences between 3xTg mice on the CD and B6129s mice on the HFD. There was no effect of time spent floating between groups for any day of the MWM. Fig. 4d depicts representative traces of swimming plots for each experimental group during the MWM probe trial.

3.4. Brain structural integrity is impaired by HFD and genotype and correlates with spatial memory measures

A total of 111 images were acquired across the 3 time points. 8 images ($n = 1$ B6129s-CD time point 3; n = 1 B6129s-HFD time point 1; $n = 2$ B6129s-HFD time point 2; n = 1 B6129s-HFD time point 3; n = 1 3xTg-CD time point 3; n = 1 3xTg-HFD time point 1; n = 1 3xTg-HFD time point 2) were removed prior to the two-level registration pipeline due to scanner artifacts or gross neuroanatomical abnormalities. The deformation-based analysis revealed a significant interaction of group and time point on local brain volume for the 3xTg-CD and

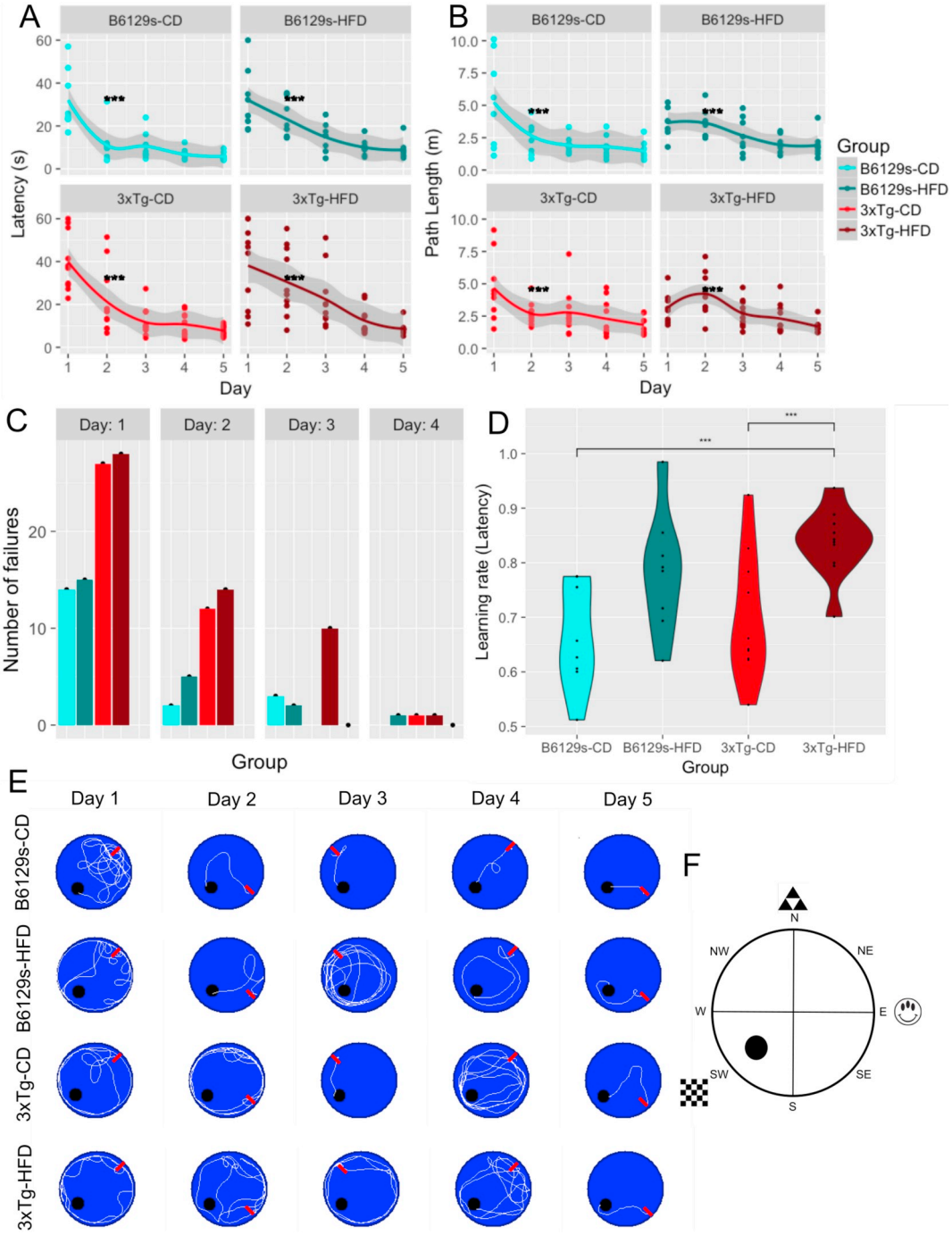

Fig. 3. MWM training days. a. Escape latencies across MWM training days. 3xTg mice on the HFD showed significantly reduced escape latencies on day 2 in comparison to B6129s mice on the CD after controlling for swim speed. **b.** Path lengths across MWM training days. 3xTg mice on the HFD showed significantly reduced path lengths on day 2 in comparison to B6129s mice on the CD. **c.** Total number of fails per group across MWM training days 1–4. **d.** Latency learning rate across MWM training days 1–5. **e.** Representative traces of swimming plots for each experimental group during MWM training days. The start position where the animal entered the pool is indicated with a red arrow. All groups were able to learn the location of the platform, as indexed by a short path length on day 5, though the B6129s-CD group was able to learn the platform location sooner and more consistently than all other groups, as indexed by a shorter path length on days 2–4. **f.** A schematic representation of the Morris water maze experimental setup. The platform was located in the SW quadrant on all training days (1-5), with distal cues located on the N, E, and SW contours of the pool. The platform was removed on the sixth day for the probe test.

3xTg-HFD groups by time point 2 and 3, and the B6129s-HFD group by time point 3, in comparison to the brain volume trajectory of the B6129s-CD group (FDR $<$ 5% for all). The mincPlotSeries function in R was used to visualize the results of the LME model on local brain volume (the log-transformed absolute Jacobians) by overlaying the t-statistics of the LME modeling results on the average anatomy background. Visualization of the interaction between time point and group is represented in Fig. 5 and suggests that the 3xTg-HFD group undergoes significant increases in local brain volume between the first and second time point (8 to 16 weeks of age) in comparison to the B6129s-CD group. However, from the second to the third time point (16 to 24 weeks of age), the 3xTg-HFD group undergoes significant decreases in local brain volume in comparison to the B6129s-CD group. Significant increases in local brain volume between the first and second

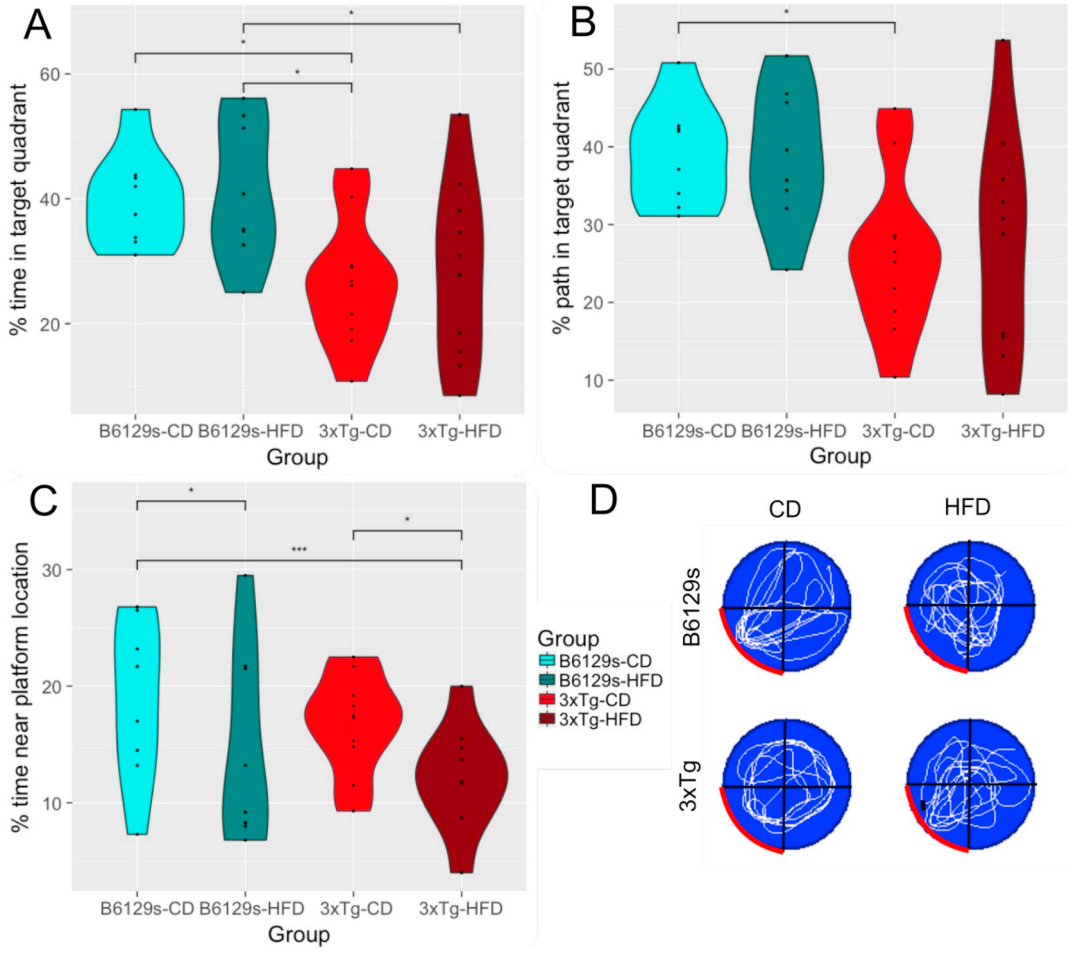

Fig. 4. MWM probe trial. a. Percent of time spent in the target quadrant on the MWM probe trial. **b.** Percent of the total path length spent in the target quadrant on the MWM probe trial. **c.** Percent of time spent near the platform location (within 2 cm) on the MWM probe trial. **d.** Representative traces of swimming plots for each experimental group during the MWM probe trial. The target quadrant (ie., the quadrant that previously contained the platform) is indicated with a red contour.

time point were also observed for the 3xTg-CD group in comparison to the B6129s-CD group, though these increases were far more localized than those occurring in the 3xTg-HFD group. Similarly, while the 3xTg-CD and B6129s-HFD groups also underwent significant decreases in local brain volume from 16 to 24 weeks in comparison to the B6129s-CD group, these decreases were not as dramatic and widespread as those evident in the 3xTg-HFD group. These results suggest that it is the additive combination of AD-like atrophy and high-fat feeding that is responsible for the enhanced distributed pattern of atrophy observed in the HFD-fed 3xTg mice, in comparison to either transgenic status or diet alone.

Further analyses subsetted the population by genotype and by dietary treatment. For both the 3xTg and B6129s genotype subsets, a significant interaction between diet and time point 3 was observed (FDR $< 5\%$). Visualization of the t-statistics of the significant interactions indicates that both 3xTg and B6129s mice on the HFD undergo significant decreases in local brain volume from 16 to 24 weeks in comparison to mice of the same respective genotype maintained on the CD (Fig. 6a), suggesting that high-fat feeding-induced obesity causes significant and widespread brain atrophy onwards of 16 weeks.

For the CD subset, there was a significant interaction between transgenic status and time point (FDR $< 5\%$), visualization of which showed slight and localized increases in local brain volume by the second time point (16 weeks) and decreases by the third time point (24 weeks) in the 3xTg-CD subset in comparison to B6129s mice maintained on the same CD (Fig. 6b). For the HFD subset, there was a significant interaction between genotype and time point 3 (FDR $<$ 5%). Visualization of results show localized increases in local brain volume by the third time point (24 weeks) in the 3xTg-HFD subset in comparison to B6129s mice maintained on the same HFD (Fig. 6b). The effect of sex was not significant for any subsetted analyses.

Furthermore, linear trends were observed between neuroanatomical volume and behavioural scores for both the percent of time (t-value = 3.66, FDR $< 15\%$) and of the total path length (t-value = 3.46, FDR $< 20\%$) spent in the target quadrant during the MWM probe trial. For both the percent time and percent of path length spent in the target quadrant, positive correlations were found in the dentate gyrus, CA1, and S1, while negative correlations were found in the piriform cortex (Fig. 6c). These correlations indicate that as the local volume of the dentate hippocampal and frontal regions increases, and that of the piriform cortex decreases, performance on a spatial memory task (the MWM) improves. The correlation between the normalized Jacobians derived from the third scanning time point (24 weeks) and the novel object discrimination ratio was not significant. There were no group x genotype interactions, suggesting that group-specific associations could not be detected and that these associations could only be generalized across genotypes.

In summary, both diet and genotype interact with time to alter neuroanatomical trajectories in comparison to B6129s mice maintained on a control diet, such that high-fat feeding seems to decrease local brain volume from 16 weeks onwards and transgenic status as a 3xTg mouse seem to decrease local brain volume by 24 weeks in mice maintained on a CD, but increase local brain volume in mice fed a HFD. Though high-fat feeding and genotype both significantly interacted

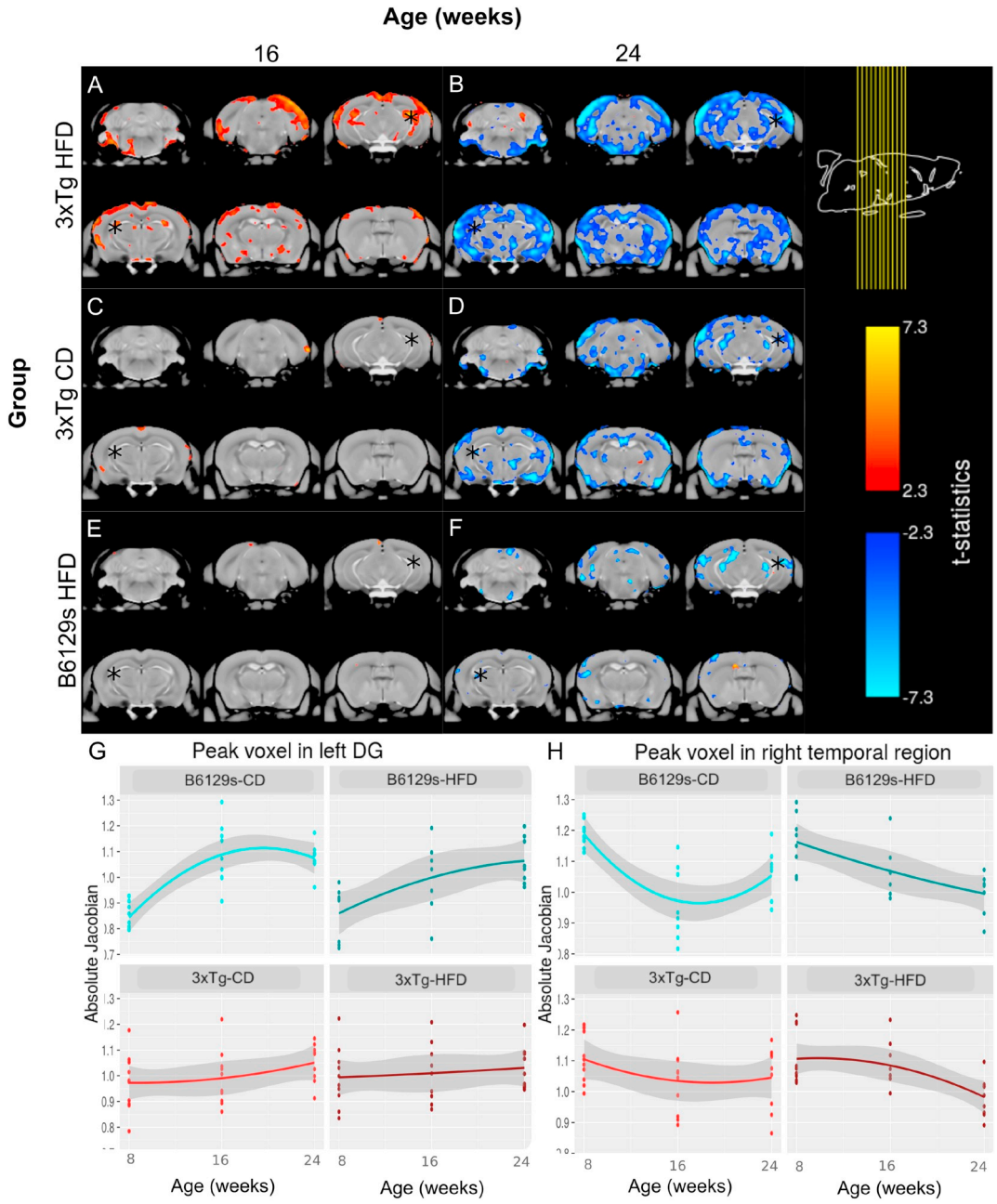

Fig. 5. Visualization of the interaction of group by time point on local brain volume (LME results) overlaid on the average anatomy background. a. 3xTg mice maintained on a HFD from 8 weeks of age undergo significant increases in local brain volume in comparison to B6129s mice fed a CD from 8 to 16 weeks, followed by dramatic and widespread decreases in brain volume (b) from 16 to 24 weeks. **c.** 3xTg mice maintained on a CD undergo initial localized increases in local brain volume, followed by distributed decreases in local brain volume **(d)** in comparison to the B6129s-CD group. **e.** B6129s mice maintained on a HFD do not undergo significant changes in local brain volume from 16 to 24 weeks in comparison to mice of the same strain maintained on a control diet, though they undergo moderate decreases from 16 to 24 weeks **(f)**. Absolute jacobians were plotted against time point for peak voxels in the left dentate gyrus (DG) **(g)** and right temporal region **(h).** The asterisks in **a-f** indicate the location of the peak voxels illustrated in **g-h**.

with time to effect local brain volume in a signature fashions, only an additive combination of HFD-induced obesity and AD-like pathology resulted in the more dramatic and widespread changes observed in the 3xTg-HFD group in comparison to the B6129s-CD group. These local brain volume changes showed putative associations with behavioural scores from the MWM probe trial, suggesting that the HFD and transgenic-related brain volume changes may be related to the mouse's performance on memory tasks. We also explored group x behaviour interactions to determine if these trajectories were group specific and found no association associations in both voxel-wise and volumetric analyses, even at lenient thresholds.

3.5. HFD alters specific neuroanatomical trajectories

5 images were removed prior to statistical analysis due to mislabeling of brain regions (n = 1 B6129s-CD time point 1, time point 2, time point 3; n = 1 3xTg-CD time point 1; n = 1 3xTg-HFD time point 3). The volumetric analysis revealed a significant group by time point interaction for a range of anatomical structures, not limited to the hippocampal region, the cingulate region, the frontal and parietal regions, the lateral septum, the olfactory bulbs, and the entorhinal cortex. The effect on many regions was differentially affected by time point, such that the interaction might be positive across the lifespan from 8 to

16 weeks of age, indicating an increase in brain volume over time in the 3xTg-HFD group in comparison to the B6129s-CD group, but negative from 16 to 24 weeks, indicating a decrease over time in the 3xTg-HFD group (or vice versa). The hippocampal region, for instance, undergoes initial bilateral increases in the 3xTg-HFD group, followed by subsequent decreases specific to the left hemisphere. Table 5 illustrates all regions with a significant interaction surviving FDR threshold of 5%. Interestingly, many of these regions are involved in the pathology of AD

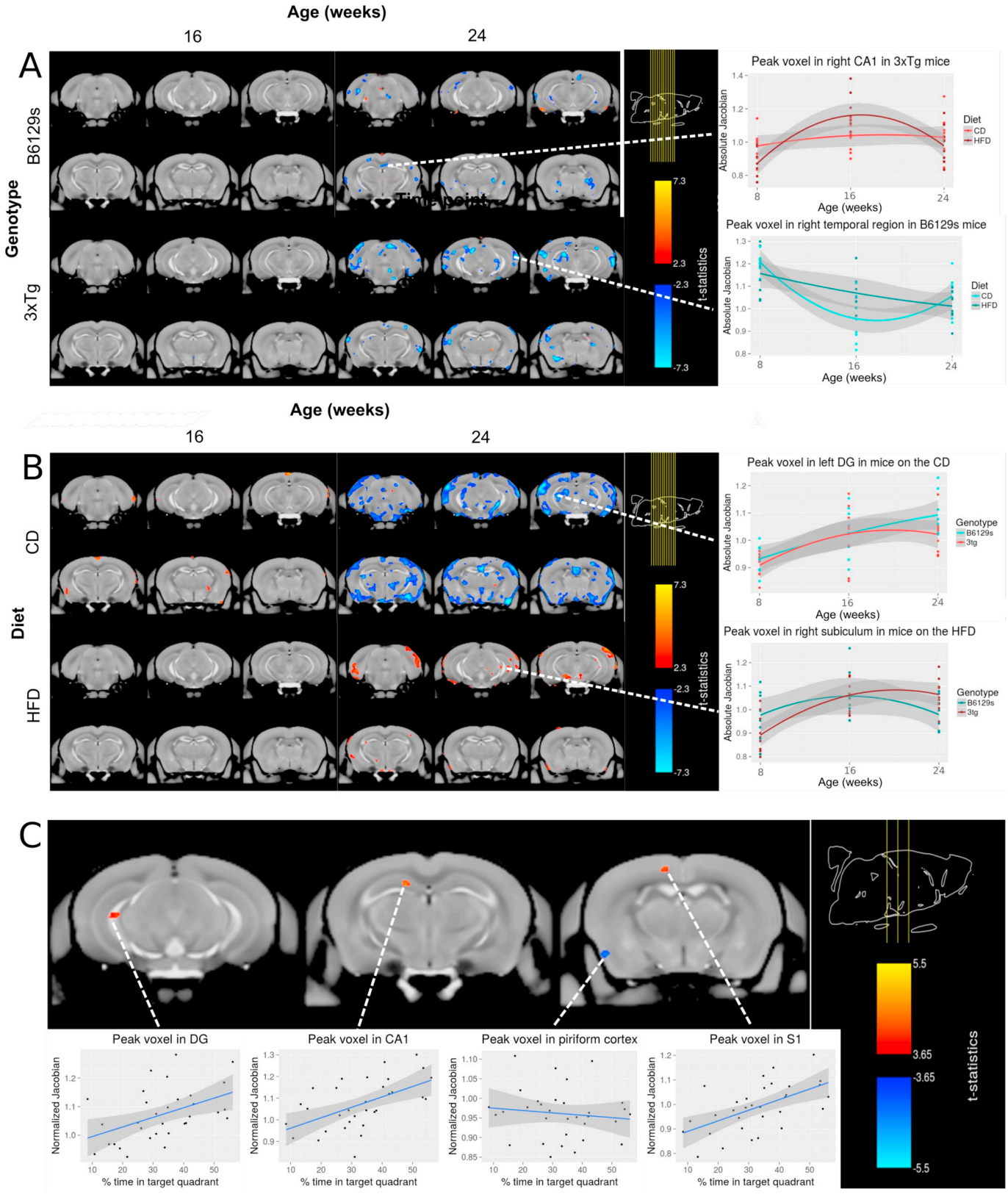

(caption on next page)

Fig. 6. Visualization of the group by time point interaction on local brain volume within genotype (panel A) and within diet condition (panel B). Association of the neuroanatomy at the final timepoint with performance in the Morris Water Maze (panel C) a. High-fat feeding has no significant effect on local brain volume from 8 to 16 weeks in B6129s and 3xTg mice, but is associated with decreases in local brain volume from 16 to 24 weeks in comparison to the CD-fed B6129s and 3xTg mice, suggesting that a HFD causes brain atrophy by 24 weeks in both genotypes. **b.** Status as a 3xTg AD-like mouse has no significant effect on local brain volume from 8 to 16 weeks in mice maintained on a control or high-fat diet, but is associated with widespread decreases in local brain volume from 16 to 24 weeks in the 3xTg-CD group in comparison to B6219s mice maintained on the CD, suggesting that AD-like pathology produced by the 3xTg mouse model causes brain atrophy by 24 weeks in mice fed the CD. The 3xTg genotype is further associated with localized increases in local brain volume from 16 to 24 weeks in the 3xTg-HFD subset in comparison to B6129s mice maintained on the HFD, suggesting that AD-like pathology produced by the 3xTg mouse model causes increases in local brain volume by 24 weeks in mice fed the HFD. **c.** Correlation between normalized Jacobians and percent of time spent in the target quadrant during the MWM probe trial. Significant positive correlations were found in the dentate gyrus, CA1, and S1, while negative correlations were found in the piriform cortex (FDR < 15%).

Table 5
MAGeT-derived brain volumes.

Group by time point 2 (16 weeks)			Group by time point 3 (24 weeks)		
Structure	**beta**	**t-value**	**Structure**	**beta**	**t-value**
Cingulate region (bilateral)	L 1.85	L 3.78	Cingulate region (bilateral)	L − 1.54	L − 3.21
	R 2.05	R 3.74		R − 1.82	R − 3.39
Frontal region (left)	3.59	3.24	Frontal region (left)	−3.94	−3.60
Hippocampal region (bilateral)	L 2.73	L 3.26	Hippocampal region (left)	−2.11	−3.57
	R 2.77	R 3.54			
Parietal region (right)	4.62	3.50	Parietal region (bilateral)	L − 4.78	L − 3.00
				R − 5.21	R − 4.12
Olfactory bulbs (bilateral)	L 2.80	L 2.85	Olfactory bulbs (bilateral)	L − 2.57	L − 2.85
	R 3.05	R 3.04		R − 2.79	R − 3.12
Occipital region (bilateral)	L 2.00	L 3.34	Occipital region (left)	−2.03	−3.46
	R 2.55	R 4.30			
Midbrain (bilateral)	3.09	3.45	Midbrain (bilateral)	−2.62	−2.96
Amygdala (right)	2.01	3.99	Amygdala (left)	−1.88	−3.75
Lateral septum (bilateral)	L 0.57	L 3.14	Fimbria (bilateral)	L − 0.52	L − 3.00
	R 0.47	R 3.27		R − 0.57	R − 3.46
Olfactory tubercle (bilateral)	L 0.53	L 3.07	Temporal region (left)	−1.38	−3.00
	R 0.49	R 2.98			
Entorhinal cortex (left)	2.17	4.21	Nucleus accumbens (left)	−0.65	−2.95
Thalamus (right)	2.19	2.97	Hypothalamus (right)	−1.12	−3.37
Cerebellar white matter (left)	−0.40	−3.22	Subiculum (left)	−0.55	−3.13
Corticospinal tract / pyramids (right)	0.34	3.18	Insular region (right)	−2.55	−4.94
Inferior olivary complex (right)	0.17	2.83	Basal forebrain (left)	−0.81	−4.41
Insular claustrum (right)	0.46	3.46	Stria terminalis (right)	−0.24	−4.53
			Lateral olfactory tract (bilateral)	L − 0.51	L − 4.13
				R − 0.33	R − 3.19
			Endopiriform claustrum (right)	−0.42	−3.22
			Anterior commissure: pars anterior (bilateral)	L − 0.40	L − 3.68
				R − 0.30	R − 3.06
			Superior olivary complex (right)	−0.21	−2.82
			Piriform cortex area (right)	−2.20	−3.89

Regions showing significant interaction for group by time point (FDR < 5%).

(hippocampus, cingulate cortex, entorhinal cortex) and are equally known to be affected by obesity (frontal lobes, cingulate gyrus, amygdala, thalamus, occipital lobe, hippocampus) in human studies.

Volumetric analyses were further subsetted by genotype and by dietary treatment. A significant diet by time point 3 interaction was observed across anatomical structures for the 3xTg subset of mice, but not for the B6129s mice, suggesting that high-fat feeding has a more profound impact on mice with AD-like pathology, as opposed to the non-transgenic control strain. For both the HFD and CD subsets of mice, a significant interaction between genotype and time point 3 was observed for multiple brain regions. An additional interaction between genotype and time point 2 was significant for mice maintained on the CD. Supplementary Tables A5–7 illustrate the brain regions with a significant interaction for the 3xTg, CD, and HFD subsets, however each of these findings survive FDR correction at > 5 to < 20%. Fig. 7 illustrates the volumetric trajectories of select regions from Table 5. Supplementary fig. A1 illustrates the volumetric trajectories of significant regions from subset contrasts listed in Supplementary tables A5–7.

4. Discussion

The present study is the first to use longitudinal MRI and behavioural assays to characterize the developmental brain-behaviour phenotype of obesity and its effect on Alzheimer's disease progression, and particularly examining these effects earlier in the lifespan. As demonstrated here and by others, the combination of longitudinal neuroimaging and behavioural analyses can provide important insights when examining preclinical models with and without treatment (Kong et al., 2018; Guma et al., 2018; Zhang et al., 2010; Lau et al., 2008). A major finding from our study is that high-fat feeding exacerbated the brain volume abnormalities and spatial memory deficits in the 3xTg mouse model in comparison to the 3xTg mice maintained on the CD. This suggests that obesity accelerates the brain atrophy and cognitive decline related to AD. Though few studies have explored the behavioural correlates of diet-induced obesity in mouse models of AD, most similarly report a detrimental effect of a HFD on memory. For instance, 12-month old female 3xTg-AD mice maintained on a HFD since 2 months of age showed impaired memory in comparison to 3xTg mice on the CD in the NOR task, though no differences were observed between HFD and CD groups in the percent alterations in the alternating Y-maze (Martin et al., 2014). Knight et al. (2014) found that high-fat feeding decreased the time spent in the target quadrant on the MWM probe trial in 3xTg mice compared with control-fed mice. Though we found that high-fat feeding did not specifically impair memory within a

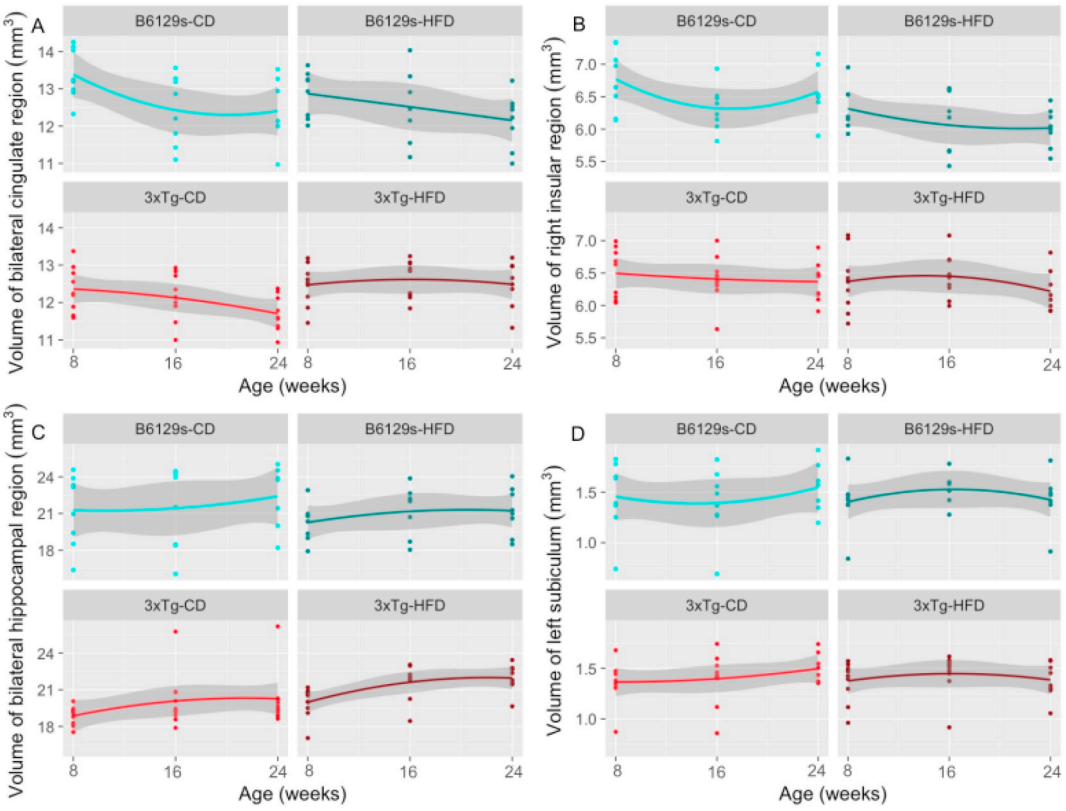

Fig. 7. MAGeT-derived volumetric trajectories across time point (quadratic). a-c show select regions with a significant interaction between group and time point for the bilateral cingulate region **(a)**, right insular region **(b)**, left subiculum **(c),** and bilateral hippocampus (plotted as average hippocampal volume) **(d)** All regions survive FDR < 5%.

genotypic group on the NOR task, this may represent a limitation of the NOR task, as opposed to a lack of a significant effect of high-fat feeding on memory in 3xTg mice, considering that 3xTg mice fed the CD were already achieving the worst possible score on the NOR. This finding may not necessarily be indicative of a poorer short-term memory in comparison to an animal with a discrimination ratio of 0. Thus, the finding that high-fat feeding did not impair memory within a genotypic group may represent a limitation of the NOR task, as opposed to a lack of a significant effect of high-fat feeding on memory in 3xTg mice. Consistent with previous work showing no diet-specific effect of high-fat feeding in 3xTg mice, Knight et al. (2014) found that 3 month old 3xTg mice showed impaired memory on the NOR, regardless of diet (HFD or CD). However, they also report that non-transgenic mice on a HFD from 2 months of age exhibited memory impairments on the NOR task in comparison to CD non-transgenic mice. Although this comparison was not significant in the present study, we observed that high-fat feeding lowered the NOR score of B6129s control mice. Beyond behavioural correlates, no animal study to date has examined the MRI-derived brain structural changes associated with the interaction of obesity with dementia progression in an AD mouse model. Human studies, however, suggest that obesity may accelerate the brain structural changes implicated in AD. A study of cognitively impaired elderly individuals found that higher BMI is associated with brain atrophy (Ho et al., 2010), and, more specifically, that higher BMI is negatively correlated with anterior hippocampal volume in patients with AD (Ho et al., 2011). Though the structural deficits induced by high-fat feeding were widespread, our volumetric analysis pinpointed specific regions encompassing these alterations, such as the hippocampal region. The hippocampus has long been observed to be one of the first brain structures affected by AD and decreased hippocampal volumes are observed in elderly healthy controls displaying the first signs of cognitive decline (Zanchi et al., 2017). Overall, our data suggest that obesity contributes to compromising the integrity of brain structure and cognitive abilities in mouse models of AD.

Another important finding of the present study is that high-fat feeding induced memory deficits and brain atrophy in control mice to a considerable extent. Indeed, in most measures of spatial and short-term memory, there were no differences between the memory and learning capabilities of B6129s mice on the HFD and 3xTg mice on the CD and HFD significantly reduced the percent of time control mice spent near the platform location in the MWM. However, this impairment of high-fat feeding was not observed for all spatial memory indices, suggesting a need to further evaluate and discern the contributions of the HFD to cognitive decline. Consistent with human and animal studies, obesity is associated with memory impairments, independently of AD. Non-transgenic mice exposed to a HFD have been shown to develop cognitive impairment, such as impairment of hippocampal-dependent learning on the radial-arm maze (Valladolid-Acebes et al., 2011) and object location memory (Heyward et al., 2012) in diet-induced obese C57BL/6 J mice. In humans, intake of a HFD is associated with deficits on cognitive tasks (Freeman et al., 2014). This highlights the detriment of obesity to the general population (independent of AD) and cautions its ability to engender memory impairments resemblant of AD.

The strengths of the current study include the longitudinal use of MRI to assess the morphological changes the brain undergoes in obesity and AD-like progression. In humans, higher BMI is associated with MRI-derived brain structural changes, such as lower gray matter density in the postcentral gyrus, frontal operculum, putamen, and middle frontal gyrus (Pannacciulli et al., 2006), as well as changes in hippocampal volume (Bobb et al., 2014). Longitudinal and cross-sectional MRI studies of AD have shown that AD is associated with regional cerebral atrophy, particularly in the hippocampus (Zanchi et al., 2017) and brain structural changes occur in mouse models of AD (Kong et al., 2018). Since both diseases (obesity and AD) can produce damage to

multiple brain regions, structural imaging is critical for characterizing this damage and constitutes an important index of neuronal health. Equally, a significant advantage of MRI is its potential to bridge human and animal studies: MRI is increasingly being used to characterize the brain structure of both humans and animals at a high level of precision, and analyses relating brain volume changes to cognitive measures or cellular changes will be pivotal to inferring the effects of obesity and other risk factors for AD in humans. Moreover, a longitudinal description of neuroanatomy is important since longitudinal studies are ultimately required to verify causality and characterize the temporal order of AD-related processes. Finally, an advantage of our study is that it correlates behaviour with changes in brain structure over time.

It bears mention that we previously performed a phenotyping study of the 3xTg AD model in Kong et al. (2018). Some of the trajectories in the 3xTg groups resemble the curvilinear differences that are observed here. However, there are key differences in the work performed in that manuscript relative to the work shown here. This includes more frequent behavioural (3 timepoints) and the MRI timepoints (6 timepoints) than what is presented in the current work. However, it may be interesting to repeat the current work with more timepoints in an effort to replicate previous work and to better understand the temporal specificity of memory and neuroanatomical degradation due to exposure to the HFD.

Our study is not without limitations. Firstly, memory was only assessed at one time point, limiting comparability of memory integrity to baseline levels. We chose a single testing period to minimize training effects and the stress induced by behavioural testing and have shown previously that there are no baseline differences in memory between 3xTg and control mice at 9 weeks of age (Kong et al., 2018). Though not in the scope of this study, future work following the trajectory of memory and brain structural impairments at late-life timepoints will be crucial to understand the full extent of the negative outcomes of high-fat feeding. Secondly, as with all studies using animal models to investigate human disease processes, a limitation of our work is that the 3xTg mouse model does not fully recapitulate Alzheimer's disease in humans. Results from studies incorporating mouse models have to be interpreted in consideration of this discrepancy. Transgenic mice are created by overproducing AD-related proteins and differences may exist in the timing and constitution of the amyloid plaques and NFT tangles (Mastrangelo and Bowers, 2008). Though human AD and mouse models thereof are not directly interchangeable, mouse models of AD replicate the relevant features of the disease and have proven invaluable to understanding the pathogenesis and treatment of AD in humans. Thirdly, though we show here that HFD-induced obesity alters the pathological changes associated with AD at the gross morphological level, no conclusions can be drawn concerning the fine-grained cellular changes that may mediate this neuroanatomical remodelling, which would require histological and immunohistochemistry experiments. Though such a mechanism remains unknown, several have been proposed, including insulin resistance, oxidative stress and chronic inflammatory processes and research suggests strong etiological overlap and shared pathophysiological abnormalities between metabolic disease (obesity, type 2 diabetes) and AD (Freeman et al., 2014; Kang et al., 2017).

By characterizing the neuroanatomical and behavioural changes associated with the impact of obesity on the pathology of AD, our work is particularly relevant towards developing preventative strategies that could modify preclinical disease-related trajectories by targeting obesity. Such strategies are especially necessary considering the lack of available treatments for AD (Cummings et al., 2014) and the limited clinical efficacy of AD pharmaceuticals (Schneider et al., 2014). Though we show here that the adolescent period is sensitive to the deleterious effects of high-fat feeding, it is equally a period with the capacity to reverse such damaging effects. Boitard et al. (2016) showed that chronic exposure to a HFD during adolescence in rats impaired hippocampal function and enhanced amygdala function, but that switching the rats to a control diet restored hippocampal neurogenesis and normalized amygdala activity. Therefore, though adolescence is vulnerable to determining long-term outcomes, it may also represent a period in which making healthy lifestyle changes can reverse incurred damages and protect against AD-related cognitive decline (Hueston et al., 2017). Promising avenues for reducing obesity include dietary modification (Walker et al., 2017), increasing levels of physical activity (Kim et al., 2016; Voss et al., 2013), and environmental enrichment. Future studies similarly characterizing the impact of other modifiable risk factors, such as smoking, hypertension, depression, among others (Barnes and Yaffe, 2011), in mouse models of AD will be integral for an improved understanding of how each interacts with AD-related pathophysiology. Equally, studies assessing the effect of interventions such as exercise, environmental enrichment, and dietary modification on lifestyle factors will be critical towards implementing public health initiatives that could tackle the intersecting obesity and Alzheimer's epidemics and dramatically decrease dementia prevalence over time.

5. Conclusion

Obesity during adolescence interacted with AD-like progression in the 3xTg mouse model of AD to exacerbate brain volume atrophy by 24 weeks and mediate alterations in neuroanatomy. Specific measures of spatial memory were impaired in HFD-fed 3xTg mice in comparison to those maintained on the CD. In fact, HFD-induced obesity aggravated memory impairment in all mice, lowering certain memory indexes of B6129s-HFD control mice to those of 3xTg mice maintained on a CD. Decline in the volumetric trajectories of hippocampal regions were associated with the degree of spatial memory impairments on the MWM paradigm at trend levels. Since brain structural integrity, as measured by MRI-derived regional brain volumes, is a useful indicator of neurological health, our work adds an important dimension to the portrait of a potentially synergistic relationship between obesity and risk for AD, as well as to the damaging effects of obesity alone. Ultimately, knowledge obtained from this study will provide insight into the brain morphological and behavioural correlates of obesity as a risk factor for AD, which will in turn help the generation of strategies aimed at reducing the risk of developing Alzheimer's.

Acknowledgements

The authors thank Axel Mathieu for his guidance in MRI acquisition and the staff of the Douglas Mental Health University Institute's Animal Facility for oustanding technical assistance.

Funding

This work was supported by Brain Canada, the Natural Sciences and Engineering Research Council of Canada, and Fonds de recherche santé Québec.

Declarations of interest

None.

Appendix A. Supplementary data

Supplementary data to this article can be found online at https://doi.org/10.1016/j.nicl.2018.11.016.

References

Alford, S., Patel, D., Perakakis, N., Mantzoros, C.S., 2017. Obesity as a risk factor for Alzheimer's disease: weighing the evidence. Obes Rev. https://doi.org/10.1111/obr.12629.

Allemang-Grand, R., et al., 2017. Neuroanatomy in mouse models of Rett syndrome is related to the severity of Mecp2 mutation and behavioral phenotypes. Mol Autism 8, 32. https://doi.org/10.1186/s13229-017-0138-8.

Amaral, R.S., et al., 2016. Manual segmentation of the fornix, fimbria, and alveus on high-resolution 3T MRI: Application via fully-automated mapping of the human memory circuit white and grey matter in healthy and pathological aging. NeuroImage. https://doi.org/10.1016/j.neuroimage.2016.10.027.

Avants, B.B., Epstein, C.L., Grossman, M., Gee, J.C., 2008. Symmetric diffeomorphic image registration with cross-correlation: evaluating automated labeling of elderly and neurodegenerative brain. Med. Image Anal. 12, 26–41. https://doi.org/10.1016/j.media.2007.06.004.

Avants, B.B., et al., 2011. A reproducible evaluation of ANTs similarity metric performance in brain image registration. NeuroImage 54, 2033–2044. https://doi.org/10.1016/j.neuroimage.2010.09.025.

Barnes, D.E., Yaffe, K., 2011. The projected effect of risk factor reduction on Alzheimer's disease prevalence. Lancet Neurol. 10, 819–828. https://doi.org/10.1016/S1474-4422(11)70072-2.

Barron, A.M., Rosario, E.R., Elteriefi, R., Pike, C.J., 2013. Sex-specific effects of high fat diet on indices of metabolic syndrome in 3xTg-AD mice: implications for Alzheimer's disease. PLoS One 8, e78554. https://doi.org/10.1371/journal.pone.0078554.

Bernal-Rusiel, J.L., et al., 2013. Statistical analysis of longitudinal neuroimage data with Linear mixed Effects models. NeuroImage 66, 249–260. https://doi.org/10.1016/j.neuroimage.2012.10.065.

Biro, F.M., Wien, M., 2010. Childhood obesity and adult morbidities. Am. J. Clin. Nutr. 91, 1499S–1505S. https://doi.org/10.3945/ajcn.2010.28701B.

Bischof, G.N., Park, D.C., 2015. Obesity and Aging: Consequences for Cognition, Brain Structure, and Brain Function. Psychosom Med 77, 697–709. https://doi.org/10.1097/PSY.0000000000000212.

Bobb, J.F., Schwartz, B.S., Davatzikos, C., Caffo, B., 2014. Cross-sectional and longitudinal association of body mass index and brain volume. Hum. Brain Mapp. 35, 75–88. https://doi.org/10.1002/hbm.22159.

Boitard, C., et al., 2012. Juvenile, but not adult exposure to high-fat diet impairs relational memory and hippocampal neurogenesis in mice. Hippocampus 22, 2095–2100. https://doi.org/10.1002/hipo.22032.

Boitard, C., et al., 2016. Switching Adolescent High-Fat Diet to Adult Control Diet Restores Neurocognitive Alterations. Front. Behav. Neurosci. 10, 225. https://doi.org/10.3389/fnbeh.2016.00225.

Chakravarty, M.M., et al., 2013. Performing label-fusion-based segmentation using multiple automatically generated templates. Hum. Brain Mapp. 34, 2635–2654. https://doi.org/10.1002/hbm.22092.

Chakravarty, M.M., et al., 2016. Deep brain stimulation of the ventromedial prefrontal cortex causes reorganization of neuronal processes and vasculature. NeuroImage 125, 422–427. https://doi.org/10.1016/j.neuroimage.2015.10.049.

Chung, M.K., et al., 2001. A unified statistical approach to deformation-based morphometry. NeuroImage 14, 595–606. https://doi.org/10.1006/nimg.2001.0862.

Cummings, J.L., Morstorf, T., Zhong, K., 2014. Alzheimer's disease drug-development pipeline: few candidates, frequent failures. Alzheimers Res. Ther. 6, 37. https://doi.org/10.1186/alzrt269.

de Flores, R., La Joie, R., Chetelat, G., 2015. Structural imaging of hippocampal subfields in healthy aging and Alzheimer's disease. Neuroscience 309, 29–50. https://doi.org/10.1016/j.neuroscience.2015.08.033.

Dean 3rd, D.C., et al., 2014. Brain differences in infants at differential genetic risk for late-onset Alzheimer disease: a cross-sectional imaging study. JAMA Neurol 71, 11–22. https://doi.org/10.1001/jamaneurol.2013.4544.

Dorr, A.E., Lerch, J.P., Spring, S., Kabani, N., Henkelman, R.M., 2008. High resolution three-dimensional brain atlas using an average magnetic resonance image of 40 adult C57Bl/6J mice. NeuroImage 42, 60–69. https://doi.org/10.1016/j.neuroimage.2008.03.037.

Eriksen, J.L., Janus, C.G., 2007. Plaques, tangles, and memory loss in mouse models of neurodegeneration. Behav. Genet. 37, 79–100. https://doi.org/10.1007/s10519-006-9118-z.

Freeman, L.R., Haley-Zitlin, V., Rosenberger, D.S., Granholm, A.C., 2014. Damaging effects of a high-fat diet to the brain and cognition: a review of proposed mechanisms. Nutr Neurosci 17, 241–251. https://doi.org/10.1179/1476830513Y.0000000092.

Friedel, M., van Eede, M.C., Pipitone, J., Chakravarty, M.M., Lerch, J.P., 2014. Pydpiper: a flexible toolkit for constructing novel registration pipelines. Front Neuroinform 8, 67. https://doi.org/10.3389/fninf.2014.00067.

Gratuze, M., et al., 2016. High-fat, high-sugar, and high-cholesterol consumption does not impact tau pathogenesis in a mouse model of Alzheimer's disease-like tau pathology. Neurobiol. Aging 47, 71–73. https://doi.org/10.1016/j.neurobiolaging.2016.07.016.

Guma, E., et al., 2018. Regional brain volume changes following chronic antipsychotic administration are mediated by the dopamine D2 receptor. NeuroImage 176, 226–238. https://doi.org/10.1016/j.neuroimage.2018.04.054.

Guyenet, S.J., Schwartz, M.W., 2012. Clinical review: Regulation of food intake, energy balance, and body fat mass: implications for the pathogenesis and treatment of obesity. J. Clin. Endocrinol. Metab. 97, 745–755. https://doi.org/10.1210/jc.2011-2525.

Heyward, F.D., et al., 2012. Adult mice maintained on a high-fat diet exhibit object location memory deficits and reduced hippocampal SIRT1 gene expression. Neurobiol. Learn. Mem. 98, 25–32. https://doi.org/10.1016/j.nlm.2012.04.005.

Ho, A.J., et al., 2010. Obesity is linked with lower brain volume in 700 AD and MCI patients. Neurobiol. Aging 31, 1326–1339. https://doi.org/10.1016/j.neurobiolaging.2010.04.006.

Ho, A.J., et al., 2011. Hippocampal volume is related to body mass index in Alzheimer's disease. Neuroreport 22, 10–14.

Hueston, C.M., Cryan, J.F., Nolan, Y.M., 2017. Stress and adolescent hippocampal neurogenesis: diet and exercise as cognitive modulators. Transl. Psychiatry 7, e1081. https://doi.org/10.1038/tp.2017.48.

Julien, C., et al., 2010. High-fat diet aggravates amyloid-beta and tau pathologies in the 3xTg-AD mouse model. Neurobiol. Aging 31, 1516–1531. https://doi.org/10.1016/j.neurobiolaging.2008.08.022.

Kang, S., Lee, Y.H., Lee, J.E., 2017. Metabolism-Centric Overview of the Pathogenesis of Alzheimer's Disease. Yonsei Med. J. 58, 479–488. https://doi.org/10.3349/ymj.2017.58.3.479.

Kim, T.W., Choi, H.H., Chung, Y.R., 2016. Treadmill exercise alleviates impairment of cognitive function by enhancing hippocampal neuroplasticity in the high-fat diet-induced obese mice. J Exerc Rehabil 12, 156–162. https://doi.org/10.12965/jer.1632644.322.

Kivipelto, M., et al., 2006. Risk score for the prediction of dementia risk in 20 years among middle aged people: a longitudinal, population-based study. Lancet Neurol. 5, 735–741. https://doi.org/10.1016/S1474-4422(06)70537-3.

Knight, E.M., Martins, I.V., Gumusgoz, S., Allan, S.M., Lawrence, C.B., 2014. High-fat diet-induced memory impairment in triple-transgenic Alzheimer's disease (3xTgAD) mice is independent of changes in amyloid and tau pathology. Neurobiol. Aging 35, 1821–1832. https://doi.org/10.1016/j.neurobiolaging.2014.02.010.

Kong, V., et al., 2018. Early-in-life neuroanatomical and behavioural trajectories in a triple transgenic model of Alzheimer's disease. Brain Struct Funct. https://doi.org/10.1007/s00429-018-1691-4.

Kuo, Y.T., Herlihy, A.H., So, P.W., Bhakoo, K.K., Bell, J.D., 2005. In vivo measurements of T1 relaxation times in mouse brain associated with different modes of systemic administration of manganese chloride. J. Magn. Reson. Imaging 21, 334–339. https://doi.org/10.1002/jmri.20285.

Lau, J.C., et al., 2008. Longitudinal neuroanatomical changes determined by deformation-based morphometry in a mouse model of Alzheimer's disease. NeuroImage 42, 19–27. https://doi.org/10.1016/j.neuroimage.2008.04.252.

Lee, J.H., Silva, A.C., Merkle, H., Koretsky, A.P., 2005. Manganese-enhanced magnetic resonance imaging of mouse brain after systemic administration of $MnCl_2$: dose-dependent and temporal evolution of T1 contrast. Magn. Reson. Med. 53, 640–648. https://doi.org/10.1002/mrm.20368.

Lerch, J., Hammill, C., Eede, M., Cassel, D., 2016. RMINC: statistical tools for medical imaging NetCDF (MINC) Files. In: R Package Version 1.3.0.0, . https://CRAN.R-project.org/package=RMINC.

Livingston, G., et al., 2017. Dementia prevention, intervention, and care. Lancet. https://doi.org/10.1016/S0140-6736(17)31363-6.

Luciano, R., et al., 2015. Biomarkers of Alzheimer disease, insulin resistance, and obesity in childhood. Pediatrics 135, 1074–1081. https://doi.org/10.1542/peds.2014-2391.

Malheiros, J.M., Paiva, F.F., Longo, B.M., Hamani, C., Covolan, L., 2015. Manganese-Enhanced MRI: Biological applications in Neuroscience. Front. Neurol. 6, 161. https://doi.org/10.3389/fneur.2015.00161.

Manjon, J.V., Tohka, J., Robles, M., 2010. Improved estimates of partial volume coefficients from noisy brain MRI using spatial context. NeuroImage 53, 480–490. https://doi.org/10.1016/j.neuroimage.2010.06.046.

Martin, S.A., Jameson, C.H., Allan, S.M., Lawrence, C.B., 2014. Maternal high-fat diet worsens memory deficits in the triple-transgenic (3xTgAD) mouse model of Alzheimer's disease. PloS One 9 (6).

Massaad, C.A., Pautler, R.G., 2011. Manganese-enhanced magnetic resonance imaging (MEMRI). Methods Mol. Biol. 711, 145–174. https://doi.org/10.1007/978-1-61737-992-5_7.

Mastrangelo, M.A., Bowers, W.J., 2008. Detailed immunohistochemical characterization of temporal and spatial progression of Alzheimer's disease-related pathologies in male triple-transgenic mice. BMC Neurosci. 9, 81. https://doi.org/10.1186/1471-2202-9-81.

Moceri, V.M., Kukull, W.A., Emanuel, I., van Belle, G., Larson, E.B., 2000. Early-life risk factors and the development of Alzheimer's disease. Neurology 54, 415–420.

Ng, M., et al., 2014. Global, regional, and national prevalence of overweight and obesity in children and adults during 1980-2013: a systematic analysis for the Global Burden of Disease Study 2013. Lancet 384, 766–781. https://doi.org/10.1016/S0140-6736(14)60460-8.

Oddo, S., Caccamo, A., Kitazawa, M., Tseng, B.P., Laferla, F.M., 2003a. Amyloid deposition precedes tangle formation in a triple transgenic model of Alzheimer's disease. Neurobiol. Aging 24, 1063–1070.

Oddo, S., et al., 2003b. Triple-transgenic model of Alzheimer's disease with plaques and tangles: intracellular Abeta and synaptic dysfunction. Neuron 39, 409–421.

Pannacciulli, N., et al., 2006. Brain abnormalities in human obesity: a voxel-based morphometric study. NeuroImage 31, 1419–1425. https://doi.org/10.1016/j.neuroimage.2006.01.047.

Petrov, D., et al., 2015. High-fat diet-induced deregulation of hippocampal insulin signaling and mitochondrial homeostasis deficiences contribute to Alzheimer disease pathology in rodents. Biochim. Biophys. Acta 1852, 1687–1699. https://doi.org/10.1016/j.bbadis.2015.05.004.

Pfefferbaum, A., et al., 2013. Variation in longitudinal trajectories of regional brain volumes of healthy men and women (ages 10 to 85 years) measured with atlas-based parcellation of MRI. NeuroImage 65, 176–193. https://doi.org/10.1016/j.neuroimage.2012.10.008.

Poole, D.S., et al., 2017. Continuous infusion of manganese improves contrast and reduces side effects in manganese-enhanced magnetic resonance imaging studies. NeuroImage 147, 1–9. https://doi.org/10.1016/j.neuroimage.2016.09.030.

Profenno, L.A., Porsteinsson, A.P., Faraone, S.V., 2010. Meta-analysis of Alzheimer's disease risk with obesity, diabetes, and related disorders. Biol. Psychiatry 67, 505–512. https://doi.org/10.1016/j.biopsych.2009.02.013.

Reichelt, A.C., 2016. Adolescent Maturational Transitions in the Prefrontal Cortex and Dopamine Signaling as a risk factor for the Development of Obesity and High Fat/High Sugar Diet Induced Cognitive Deficits. Front. Behav. Neurosci. 10, 189. https://doi.org/10.3389/fnbeh.2016.00189.

Reinert, K.R., Po'e, E.K., Barkin, S.L., 2013. The relationship between executive function

and obesity in children and adolescents: a systematic literature review. Journal of obesity 2013, 820956.
Ronan, L., et al., 2016. Obesity associated with increased brain age from midlife. Neurobiol. Aging 47, 63–70. https://doi.org/10.1016/j.neurobiolaging.2016.07.010.
Sawyer, S.M., et al., 2012. Adolescence: a foundation for future health. Lancet 379, 1630–1640. https://doi.org/10.1016/S0140-6736(12)60072-5.
Schneider, L.S., et al., 2014. Clinical trials and late-stage drug development for Alzheimer's disease: an appraisal from 1984 to 2014. J. Intern. Med. 275, 251–283. https://doi.org/10.1111/joim.12191.
Seifan, A., Schelke, M., Obeng-Aduasare, Y., Isaacson, R., 2015. Early Life Epidemiology of Alzheimer's Disease–a critical Review. Neuroepidemiology 45, 237–254. https://doi.org/10.1159/000439568.
Seo, Y., et al., 2011. Mn-bicine: a low affinity chelate for manganese ion enhanced MRI. Magn. Reson. Med. 65, 1005–1012. https://doi.org/10.1002/mrm.22680.
Shaw, P., et al., 2007. Cortical morphology in children and adolescents with different apolipoprotein E gene polymorphisms: an observational study. Lancet Neurol. 6, 494–500. https://doi.org/10.1016/S1474-4422(07)70106-0.
Silva, A.C., Bock, N.A., 2008. Manganese-enhanced MRI: an exceptional tool in translational neuroimaging. Schizophr. Bull. 34, 595–604. https://doi.org/10.1093/schbul/sbn056.
Simmonds, M., Llewellyn, A., Owen, C.G., Woolacott, N., 2016. Predicting adult obesity from childhood obesity: a systematic review and meta-analysis. Obes. Rev. 17, 95–107. https://doi.org/10.1111/obr.12334.
Steadman, P.E., et al., 2014. Genetic effects on cerebellar structure across mouse models of autism using a magnetic resonance imaging atlas. Autism Res. 7, 124–137. https://doi.org/10.1002/aur.1344.
Tardif, C.L., et al., 2018. Regionally specific changes in the hippocampal circuitry accompany progression of cerebrospinal fluid biomarkers in preclinical Alzheimer's disease. Hum. Brain Mapp. 39, 971–984. https://doi.org/10.1002/hbm.23897.
The, N.S., Suchindran, C., North, K.E., Popkin, B.M., Gordon-Larsen, P., 2010. Association of adolescent obesity with risk of severe obesity in adulthood. JAMA 304, 2042–2047. https://doi.org/10.1001/jama.2010.1635.
Ullmann, J.F., et al., 2014. An MRI atlas of the mouse basal ganglia. Brain Struct. Funct. 219, 1343–1353. https://doi.org/10.1007/s00429-013-0572-0.
Valladolid-Acebes, I., et al., 2011. High-fat diets impair spatial learning in the radial-arm maze in mice. Neurobiol. Learn. Mem. 95, 80–85. https://doi.org/10.1016/j.nlm.2010.11.007.
Vandal, M., et al., 2014. Insulin reverses the high-fat diet-induced increase in brain Abeta and improves memory in an animal model of Alzheimer disease. Diabetes 63, 4291–4301. https://doi.org/10.2337/db14-0375.
Voineskos, A.N., et al., 2015. Hippocampal (subfield) volume and shape in relation to cognitive performance across the adult lifespan. Hum. Brain Mapp. 36, 3020–3037. https://doi.org/10.1002/hbm.22825.
Voss, M.W., Vivar, C., Kramer, A.F., van Praag, H., 2013. Bridging animal and human models of exercise-induced brain plasticity. Trends Cogn. Sci. 17, 525–544. https://doi.org/10.1016/j.tics.2013.08.001.
Vousden, D.A., et al., 2018. Continuous manganese delivery via osmotic pumps for manganese-enhanced mouse MRI does not impair spatial learning but leads to skin ulceration. NeuroImage 173, 411–420. https://doi.org/10.1016/j.neuroimage.2018.02.046.
Walker, J.M., Dixit, S., Saulsberry, A.C., May, J.M., Harrison, F.E., 2017. Reversal of high fat diet-induced obesity improves glucose tolerance, inflammatory response, beta-amyloid accumulation and cognitive decline in the APP/PSEN1 mouse model of Alzheimer's disease. Neurobiol. Dis. 100, 87–98. https://doi.org/10.1016/j.nbd.2017.01.004.
Whitmer, R.A., et al., 2008. Central obesity and increased risk of dementia more than three decades later. Neurology 71, 1057–1064. https://doi.org/10.1212/01.wnl.0000306313.89165.ef.
Xu, W.L., et al., 2011. Midlife overweight and obesity increase late-life dementia risk: a population-based twin study. Neurology 76, 1568–1574. https://doi.org/10.1212/WNL.0b013e3182190d09.
Yau, P.L., Castro, M.G., Tagani, A., Tsui, W.H., Convit, A., 2012. Obesity and metabolic syndrome and functional and structural brain impairments in adolescence. Pediatrics 130, e856–e864. https://doi.org/10.1542/peds.2012-0324.
Zanchi, D., Giannakopoulos, P., Borgwardt, S., Rodriguez, C., Haller, S., 2017. Hippocampal and Amygdala Gray Matter loss in elderly Controls with Subtle Cognitive Decline. Front. Aging Neurosci. 9, 50. https://doi.org/10.3389/fnagi.2017.00050.
Zhang, J., et al., 2010. Longitudinal characterization of brain atrophy of a Huntington's disease mouse model by automated morphological analyses of magnetic resonance images. NeuroImage 49, 2340–2351. https://doi.org/10.1016/j.neuroimage.2009.10.027.
Ziegler, G., Dahnke, R., Gaser, C., 2012. Alzheimer's Disease Neuroimaging, I. Models of the aging brain structure and individual decline. Front Neuroinform 6 (3). https://doi.org/10.3389/fninf.2012.00003.